Temporal characterization of laser-induced plasma of tungsten in air

Eshita Mal[1], Rajendhar Junjuri[2], Manoj Kumar Gundawar[2] and Alika Khare[1]

[1]Indian Institute of Technology Guwahati, Guwahati, India and [2]Advanced Centre of Research in High Fluence Materials, University of Hyderabad, Hyderabad, India

Abstract

In this manuscript, the time-resolved laser-induced breakdown spectroscopy (LIBS) on tungsten target in air and the coexistence of LTE among atoms and ions as well as the fulfillment of optically thin plasma condition are reported. The laser-induced plasma (LIP) of tungsten is generated by focusing the second harmonic of a Q-switched Nd:YAG laser of pulse width ∼7 ns and repetition rate of 1 Hz on the tungsten target. The temporal evolution of LIP of tungsten is recorded at four different incident laser fluences of 60, 120, 180, and 270 J/cm^2. The several atomic and singly ionized lines of tungsten are identified in LIP. For the estimation of plasma temperature via the Boltzmann plot, the transitions at 430.7, 449.4, 468.0, 484.3, 505.3, and 524.2 nm of Atomic transition of tungsten (WI) and that of the ionic transitions, First Ionic transition of Tungsten (WII) at 251.0, 272.9, and 357.2 nm are selected. The electron density is estimated using the Stark-broadened profile of WI line at 430.2 nm. The McWhirter criteria for the local thermodynamic equilibrium (LTE) condition is verified in present experimental conditions as well as the relaxation time and diffusion length are estimated to take into account the transient and inhomogeneous nature of the plasma. The optically thin plasma condition is studied by assessing the experimental intensity ratio of atomic lines and compared with that of the theoretical intensity ratio (branching ratio). The signal to noise ratio (SNR) is also obtained as a function of time with respect to laser pulse and incident laser fluence. All these observations indicate that the spectra should be recorded within the temporal window of 1–3.5 μs with respect to laser pulse where the plasma can be treated as optically thin as well as under LTE simultaneously along with the large SNR.

Introduction

The focusing of high power pulsed laser on to a sample generates a high-temperature and high-density laser-induced plasma (LIP) (Russo, 1995). The focus on LIP is not only on the basic scientific research but also its diverse range of applications in various domains, which includes pulsed laser deposition (Lowndes *et al.*, 1996), a source of shorter wavelength radiation (Chenais-Popovics *et al.*, 1996; White *et al.*, 2007), nanoparticle generation (Amoruso *et al.*, 2005; Eliezer *et al.*, 2005), high-order harmonic generation (HHG) (Ganeev, 2007; Thaury and Quéré, 2010), micromachining (Dellasega *et al.*, 2012), and laser cleaning (Afif *et al.*, 1996). The characterization of LIP is strongly dependent upon several experimental parameters, including laser parameters [laser energy (Akram *et al.*, 2014; Zhang *et al.*, 2014), pulse duration (Le Drogoff *et al.*, 2004), wavelength (Harilal *et al.*, 2011; Díaz *et al.*, 2018), and laser spot size (Li *et al.*, 2013; Cortez *et al.*, 2017)], the physical–chemical properties of target material (Cabalin and Laserna, 1998), laser focusing geometry (Multari *et al.*, 1996), and the nature and pressure of ambient gases (Harilal *et al.*, 2006; Zehra *et al.*, 2017). The LIP is highly exuberant in nature and its parameters vary drastically with distance from the target surface both along the plume expansion direction (axial) and orthogonal to plume expansion directions (radial) as well as with time immediately after the onset of its commencement (Lazzari *et al.*, 1994; Ershov-Pavlov *et al.*, 2008). Therefore, the characterization and detailed understanding of LIP is a challenging task. The conventional plasma characterization technique employed for the estimation of plasma parameters (temperature and electron density) are optical emission spectroscopy (OES), the Langmuir probe, microwave and laser interferometry, and Thomson scattering. Laser-induced breakdown spectroscopy (LIBS) and OES are a relatively simple but a versatile technique and used for qualitative and quantitative analysis. There are several advantages of LIBS over other techniques (Winefordner *et al.*, 2004; Mal *et al.*, 2019), such as applicable to any sample irrespective physical states, free from any sample preparation, nearly nondestructive, simultaneous detection of multi-elemental sample, remote operation, and single-shot measurement for rapid analysis, capable of depth profiling. Owing to all these unique features, LIBS is finding its applications almost in every field of science (Bauer and Buckley, 2017). In LIBS, the light emitted from LIP during its expansion is dispersed via a spectrometer and the spectrum is recorded by a suitable photo detector.

By analyzing this spectrum, it is possible to retrieve LIP properties (temperature and density). In the present study, the tungsten target is ablated using a nanosecond laser pulse, and the LIP is studied using the time-resolved LIBS technique. Tungsten is being considered as one of the important materials used in-vessel components of thermonuclear reactors (Pitts *et al.*, 2017). Its various properties, such as high thermal conductivity and melting point (Davis *et al.*, 1998), low tritium retention (Philipps, 2011; Brezinsek *et al.*, 2013), sputtering yield (Federici *et al.*, 2005), erosion rate (Bolt *et al.*, 2004), and high neutron load capacity (Fukuda *et al.*, 2013), make this metal a suitable candidate for plasma-facing components (PFCs) in the fusion reactor (Neu *et al.*, 2013; Suslova *et al.*, 2015). During the operating condition inside the fusion vessel, several kinds of complex phenomenon take place between the plasma and inner walls of the vessel (Almaviva *et al.*, 2012; Philipps *et al.*, 2013). Due to plasma-material interaction, the erosion and deposition take place on PFC (Farid *et al.*, 2013). The deposition layer enhances the fuel retention of PFC and its properties, which in turn deteriorate the performance of the fusion reactor. The deposited amount should be below so as not to affect its performance (Mercadier *et al.*, 2011). To maintain the high performance and safety of fusion reactor, there is an active need for monitoring deposited materials on PFC and in order to implement its appropriate cleaning. At present, the offline method is employed to study the thickness of the deposited material and its composition, but these are the time-integrated effect (Mercadier *et al.*, 2011). So there is a requirement of online monitoring of PFC to explore the plasma-material interaction to maintain the high performance of the fusion reactor. For this purpose, LIBS is being considered to be a suitable online technique for analysis of composition and quantification of the plasma facing materials Plasma facing material (PFMs) (Kubkowska *et al.*, 2009; Mercadier *et al.*, 2011; Harilal *et al.*, 2013; Piip *et al.*, 2015). Besides its utility in nuclear reactor, laser ablation of tungsten using a Nd:YAG nanosecond pulsed laser is finding its various applications, such as the deposition of high-quality thin films (Mostako *et al.*, 2011; Dellasega *et al.*, 2012) and the fabrication of micro/nanostructures of compound element of tungsten (WO_3, WS_2, etc.) (Kawakami and Ozawa, 2002), which is used for sensor and optoelectronics devices (Wang *et al.*, 2012). All these applications of LIP are strongly dependent on its dynamics of plasma parameters. Therefore, the detailed knowledge about the LIP evolution to understand the mechanism involved in laser-target and laser-plasma interaction is very much required for optimizing experimental parameters for cost-effective implementation (Fu *et al.*, 2016). But there is a scarcity of the reported literature and lack of database in atomic parameters.

Therefore, in the present work, the time evolution of the LIP of tungsten is reported as a function of incident laser fluence in air. From LIP spectra of tungsten, several atomic and ionic transitions are identified. The plasma temperature is estimated using the Boltzmann plot method by carefully selecting the atomic and ionic lines to achieve higher accuracy. All the selected atomic and ionic lines have the highest upper energy level spread among them and the transition probabilities are low enough in order to neglect the self-absorption. The electron density is obtained from the Stark-broadened profile of atomic tungsten line at 430.2 nm. Both these plasma parameters are studied as a function of time with respect to laser pulse and incident laser fluence. The temporal window is identified for the existence of optically thin plasma as well as the LTE conditions at all the laser

fluence employed in the present case. The branching ratio method is applied to verify the optical thin condition in LIP. Assuming the LIP to be stationary and homogeneous, the McWhirter criteria is employed to estimate the minimum required electron density to maintain LTE. In order to take care of the transient and inhomogeneous nature of the LIP, the relaxation time and diffusion length are also estimated to ensure LTE in such a situation.

Experimental setup

The schematic diagram of the experimental setup used in the present work for time-resolved LIBS studies on tungsten is shown in Figure 1a. In brief, the experimental work is performed in air by focusing a Q-switched Nd:YAG laser (INNOLAS Split light 1200), operating at the second harmonic (wavelength 532 nm), pulse width ~7 ns and repetition rate of 1 Hz on the tungsten target having purity of 99.95% (Alfa Aesar) at normal incidence to generate the LIP of tungsten. The focal length of the lens used to focus the laser beam is 15 cm. This gives the beam spot size of ~230 μm on the sample as measured by an optical microscope (OLYMPUS BX51M) from a single-shot laser-ablated surface. The experiment is performed at four different laser energies of 25, 50, 75, and 100 mJ corresponding to the fluence of 60, 120, 180, and 270 J/cm^2, respectively, on to the surface of the target. The tungsten target is being translated across the laser beam in order to avoid any pitting or the formation of deep crater so as to provide the fresh surface for ablation on a shot-to-shot basis. The plasma radiation is collected at 45° with the incident laser beam by a system of collection optics and transmitted through an optical fiber, to the entrance of an echelle spectrometer (Andor Mechelle ME5000) having resolution of 0.01 nm. The echelle spectrometer equipped with intensified charge couple device (ICCD) is capable of recording the spectrum over a wide spectral range of 200–850 nm in a one single-shot acquisition. The ICCD is operated in a gated mode to record the spectra as a function of time with respect to the laser pulse in the temporal range of 0.5–5 μs by maintaining the gate width fixed at 0.5 μs duration. To trigger the ICCD at different delay times with respect to laser pulse, a delay generator (Stanford Research Systems DG545) is triggered with the Pockels cell output of the laser and a desirable delayed Transistor–transistor logic (TTL) (0–5 V) pulse is generated to trigger the ICCD. To monitor the arrival of the laser pulse and the opening of the ICCD, a part of the laser beam is detected by a photodiode and is displayed on a DSO (Tektronix TDS 2024B) simultaneously along with the ICCD gate delay. This timing scheme used in the present experimental setup to trigger the ICCD detector at the desired delay time is shown in Figure 1b. In order to improve both the SNR and the reproducibility, each and every spectrum is accumulated over 10 consecutive laser pulses and averages out.

Results and discussion

Whenever the focused laser intensity is above the breakdown threshold of the material, ablation occurs and leads to the formation of high-density, high-temperature transient inhomogeneous plasma. Due to the transient and inhomogeneous nature of the plasma, the plasma parameters change drastically both in space and time. In the following sections, the temporal evolution of plasma emission, temperature and electron density in LIP of tungsten as a function of laser fluence are described.
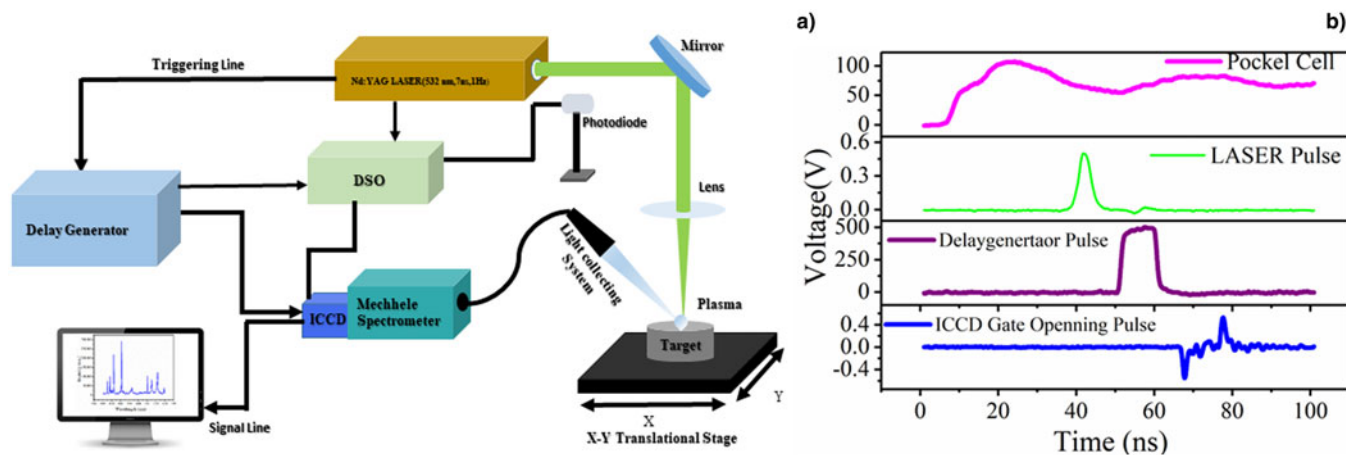
Fig. 1. (a) Schematic of the experimental setup for recording the temporal evolution of LIP of tungsten in air and (b) timing scheme for ICCD triggering.
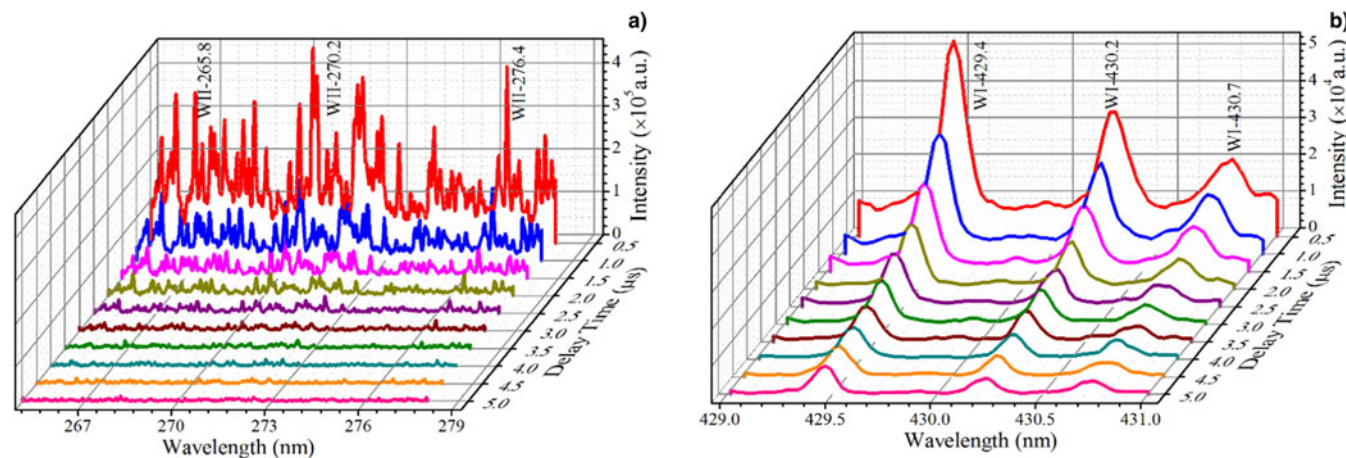

Fig. 2. Expanded view of the temporal evolution: (a) ionic (267–277 nm) and (b) atomic transitions (429–431 nm) at 60 J/cm^2 of laser fluence.

LIP emission from tungsten

The LIP spectra of tungsten in air for incident laser fluence of 60 J/cm^2 in the spectral range of 220–850 nm are shown in Figure 2 as a function of delay with respect to the laser pulse. From this, several atomic and ionic transitions of tungsten are identified using NIST and Kurucz database (https://www.nist.gov; https://www.cfa.harvard.edu/amp/ampdata/kurucz23/sekur.html). In the UV spectral range of 200–300 nm, the spectra are dominated by ionic transitions, whereas in the visible range of 300–850 nm, the emitted spectral lines are attributed to mainly atomic transitions. The expanded view of the temporal variation of the spectra in the range of 267–277 and 429–431 nm is shown in Figure 3a and 3b, respectively, at a laser fluence of 60 J/cm^2. As an example, the lines of WII at 265.8, 270.2, 258.9, and 276.4 nm are marked in Figure 3a and that of the neutral atomic lines of WI at 429.4, 430.2, and 430.7 nm in Figure 3b. The temporal evolution of the WII line at 276.4 nm and the WI line at 430.2 nm for all the fluences are shown in Figure 4a and 4b, respectively. From these, the decay time of atomic and ionic species are assessed by exponential fitting the respective data and is shown by solid lines in Figure 4. The decay time of ionic

and atomic lines is the time over which the initial intensity fall down to a 1/e factor. The variation in decay time for ionic and atomic transitions as a function of incident laser fluence is shown in Figure 5a. From this figure, it is observed that the decay time for the ionic line is 0.60 (±0.02), 0.84 (±0.04), 1.06 (±0.03), and 1.02 (±0.04) μs and that of the atomic line is 1.26 (±0.03), 1.63 (±0.09), 1.65 (±0.01), and 1.59 (±0.09) μs at four incident laser fluences of 60, 120, 180, and 270 J/cm^2, respectively. The decay time for atomic and ionic lines increases with the increase in laser fluence up to 180 J/cm^2, and then, there is a marginal fall in it. Initially, with the increase in laser fluence, the mass ablation increases up to the laser fluence of 120 J/cm^2, but at higher laser fluence of 180 J/cm^2, the mass ablation of the target decreases due to the plasma shielding at higher laser fluence (Harilal *et al.*, 1997; Haq *et al.*, 2015), resulting in the decrease in the intensity of both the atomic and ionic lines as well as their decay time. The ions possess kinetic energy than atoms and recombine with the electrons to form atoms and thus decay faster than atoms.

The signal-to-noise ratio (SNR) of the spectra is estimated using the WI at 430.2 nm transition, by the following equation
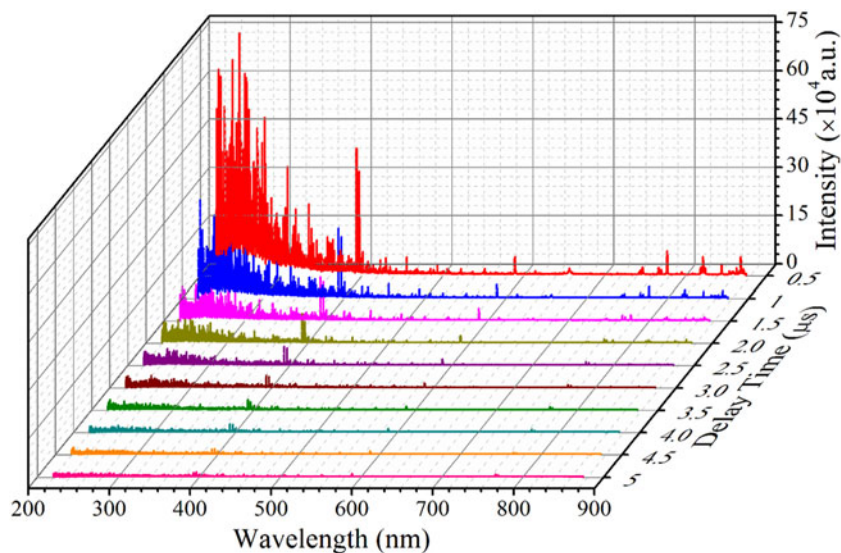
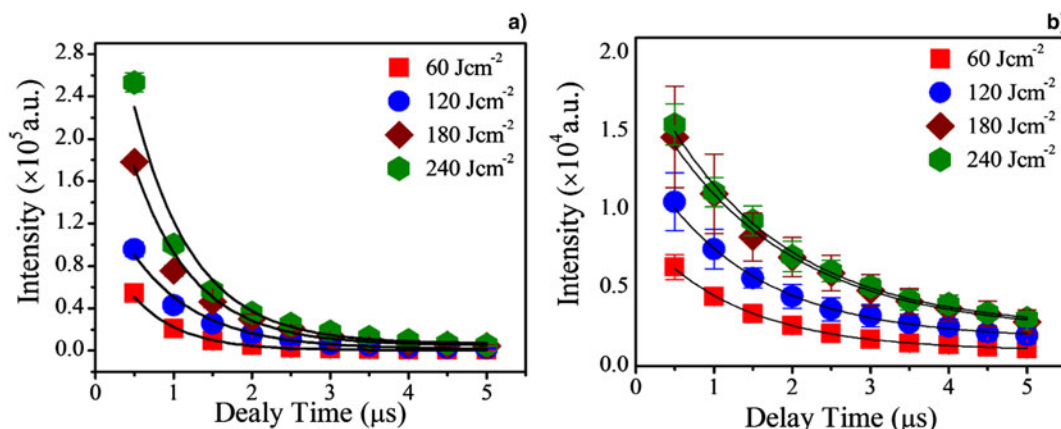**Fig. 3.** Temporal evolution of the LIP emission of tungsten in air at the laser fluence of 60 J/cm².

Fig. 4. Exponential decay of (a) WII at 276.4 nm and (b) WI at 430.2 nm at four incident laser fluences.
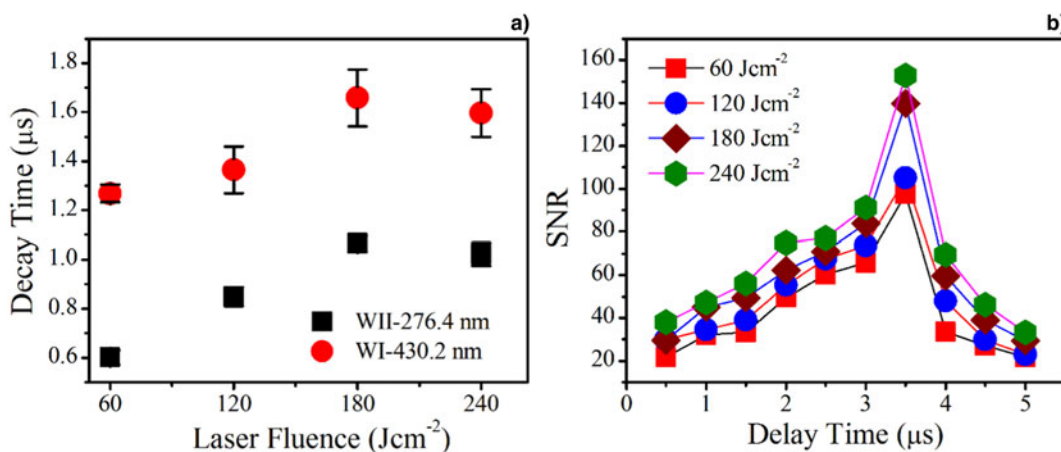

Fig. 5. (a) Decay time for the ionic and atomic tungsten line at 276.4 and 430.2 nm, respectively, with respect to laser fluence and (b) SNR for 430.2 nm line at four laser fluences as a function of delay time.

(Freeman *et al.*, 2014; Skrodzki *et al.*, 2016):

$$\text{SNR} = \frac{I_{\max} - I_{\text{background}}}{\sigma_{\text{background}}} \qquad (1)$$

where $I_{\max}$ is the integrated peak intensity for the WI at 430.2 nm line, $I_{\text{background}}$ is the averaged background intensity in the neighborhood of the line under consideration, and $\sigma_{\text{background}}$ is the standard deviation in the background intensity. The temporal

variation of the SNR of the spectra at all the laser fluence is shown in Figure 5b. It is observed that SNR increases with the delay time up to 3.5 μs for all the laser fluence and then starts falling down, similar behavior is found for the other lines too. This is due to the fact that during the initial stage of plasma formation, continuum radiation is dominated and at a later time, the intensity of emitted lines falls down (De Giacomo and Hermann, 2017). This confirms that for LIBS detection, there is a need to record the spectrum at an appropriate temporal window where the SNR is maximum.

Plasma temperature and electron density

The most widely used method to determine the plasma temperature in LIP is the Boltzmann plot method. In this, plasma is assumed to be in local thermodynamic equilibrium (LTE) and optically thin. In LTE, the line intensity of a transition, I_{nm}, from an upper level n to the lower level m is related to the upper energy state E_n, and is given by the following relation (Zhang *et al.*, 2014; Gao *et al.*, 2015):

$$\ln\left(\frac{I_{nm}\lambda_{nm}}{g_n A_{nm}}\right) = -\frac{1}{k_B T_e}E_n + \ln\left(\frac{hcN}{4\pi U(T_e)}\right) \quad (2)$$

where λ_{nm} is the wavelength of the radiation emitted due to the transition from the upper level n to the lower level m, g_n is the statistical weight of the upper level, A_{nm} is the transition probability, k_B is the Boltzmann constant, T_e is the plasma temperature, h is the Planck constant, c is the velocity of light, and N and $U(T_e)$ are the number density and partition function of the element under consideration. The plot of the left-hand side of the equation against E_n for several number of transitions is a straight line. The temperature of the species can be thus obtained from the slope of the equation, that is, $1/k_B T_e$ without the involvement of any partition function. The accuracy of temperature measurement from the Boltzmann plot method depends on the selection of the lines. The selection criteria are (1) the line's transition probability

should be low so as to neglect the self-absorption, (2) the lines should not be a resonant line (terminating to the ground state), and (3) spread in the upper energy level as large as possible. The plasma temperature for the LIP of tungsten is estimated using atomic transitions and ionic transitions. The six atomic lines at 430.7, 449.4, 468.0, 484.3, 505.3, and 524.2 nm and that of the three ionic lines at 251.0, 227.9, and 357.2 nm are selected for the estimation of plasma temperature from Eq. (2). The upper energy levels of all these selected lines for the Boltzmann plot are widely apart, and all these possess low values of transition probability. All the WI lines are non-resonant lines. The spectroscopic parameters required for these ionic and atomic transitions are taken from Kurucz database (https://www.cfa.harvard.edu/amp/ampdata/kurucz23/sekur.html) and NIST database (https://www.nist.gov), respectively, and are listed in Tables 1 and 2, respectively.

The Boltzmann plot for WII at a delay time of 0.5, 3.0, and 5.0 μs for the laser fluence of 60 J/cm² shown in Figure 6a–6c and that of the WI lines in Figure 7a–7c, respectively, as an example. The correlation coefficient for the fitted straight line by Eq. (2), for the measurement of the temperature, is found to be in the range of 0.98–0.99. The high-value correlation coefficient in the Boltzmann plot indicate the absence of self-absorption in LIP. The variation in plasma temperature as a function of delay time for all the four laser fluences estimated from ionic and atomic transitions are shown in Figure 10a and 10b, respectively. It is observed that with the delay time, the plasma temperature decreases but increases with the increase of incident laser fluence in both the cases. It is found that the plasma temperature from WII lines is higher than that of neutral atom in the delay time range of 0.5–1 μs, but at a later time and in the temporal window of 1.5–4.0 μs, both the temperatures are nearly same indicating the coexistence of thermal equilibrium among tungsten atoms and ions. During an early phase of plasma evolution, LIP mainly consists of highly energetic ions having higher kinetic energy, and thus, the temperature value is higher compared with that of atoms in the early phase of LIP, indicating the nonexistence of LTE

Table 1. Spectroscopic parameters for WII lines for the Boltzmann plot

Wavelength λ (nm)	Transition probability $(A_{nm}) \times 10^7$	Lower-level energy (E_m) (eV)	Lower-level configuration	Upper-level energy (E_n) (eV)	Upper-level configuration	g_m	g_n
251.0	4.219	2.634	5d⁵4G	7.301	–	10	12
272.9	4.272	1.095	6sa4P	5.635	5d4(5D)6p	2	2
357.2	2.207	1.313	6sa4P	4.728	6pz2S	4	2

Table 2. Spectroscopic parameters for WI lines for the Boltzmann plot

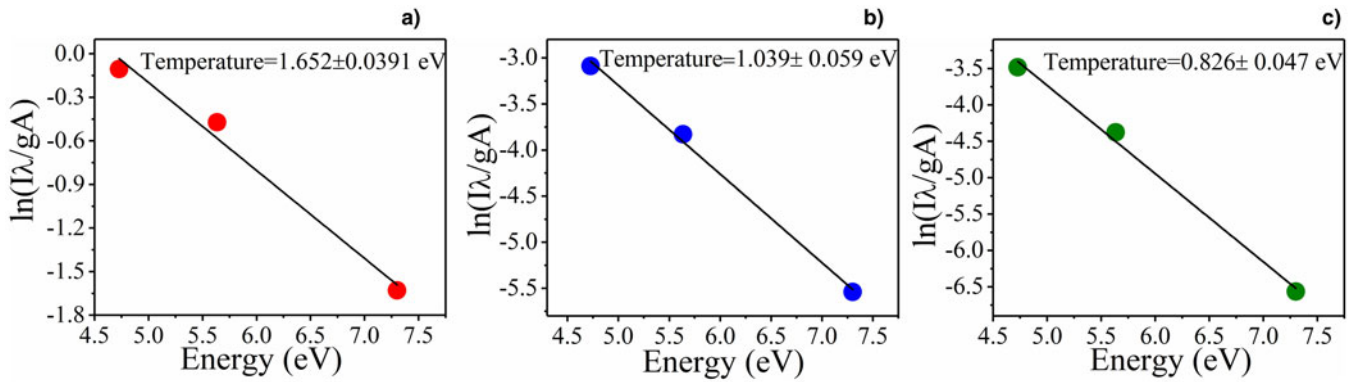| Wavelength λ (nm)	Transition probability $(A_{nm}) \times 10^6$	Lower-level energy (E_m) (eV)	Lower-level configuration	Upper-level energy (E_n) (eV)	Upper-level configuration	g_m	g_n
430.7	5.40	2.458	5d⁴6s²	5.335	–	11	11
449.4	3.00	2.387	5d⁵(⁴G)6s	5.145	–	9	7
468.0	1.40	0.598	5d⁴6s²	3.247	5d⁴6s(⁶D)6p	7	7
484.3	1.90	0.421	5d⁴6s²	2.971	5d⁴6s(⁶D)6p	5	5
505.3	1.90	0.207	5d⁴6s²	2.659	5d⁴6s(⁶D)6p	3	3
524.2	1.10	2.037	5d⁴6s²	4.401	–	9	7

Fig. 6. Boltzmann plot for WII lines at a delay time of (a) 0.5, (b) 3.0, and (c) 5.0 μs for the incident laser fluence of 60 J/cm².
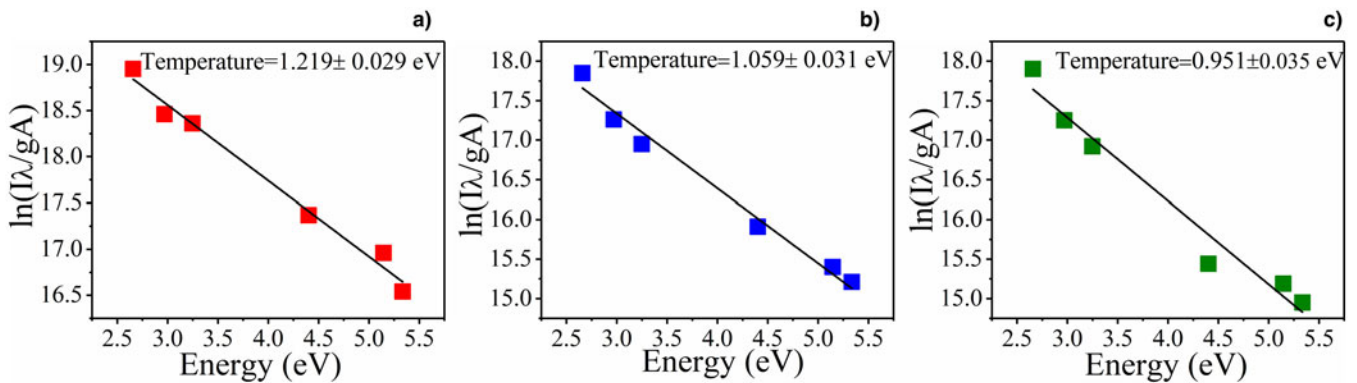

Fig. 7. Boltzmann plot for WI lines at a delay time of (a) 0.5, (b) 3.0, and (c) 5.0 μs for the incident laser fluence of 60 J/cm².

among WII and WI lines (Aguilera and Aragón, 2004). It is found that plasma temperature from WII lines varies from 1.622–0.840 (±0.034), 1.696–0.985 (±0.033), 1.805–1.001 (±0.045), and 1.913–1.182 (±0.044) eV and that for WI lines from 1.208–0.971 (±0.042), 1.304–0.985 (±0.041), 1.308–1.104 (±0.042), and 1.312–1.094 (±0.035) eV as the delay time increases from 0.5 to 5 μs at four incident laser fluences of 60, 120, 180 and 270 J/cm², respectively. In general, there is an increase in plasma temperature with the laser fluence.

The electron density of plasma is extracted using the Stark-broadened profile of the spectral line and given by (Radziemski and Cremers, 2006; Singh and Thakur, 2007; Haq *et al.*, 2015; Wermer *et al.*, 2018)

$$\Delta\lambda_{1/2} = 2w\left(\frac{N_e}{10^{16}}\right) + 3.5A\left(\frac{N_e}{10^{16}}\right)^{1/4}[1 - 1.2N_D^{-1/3}]\left(\frac{N_e}{10^{16}}\right) \quad (3)$$

where $\Delta\lambda_{1/2}$ is the full-width at half-maximum, N_e is the electron number density, w and A are the electron impact width and ion broadening parameter, respectively, and N_D is the number of particles in the Debye sphere. Considering the small contribution of ion to Stark-broadening, Eq. (3) simplifies to the following (Cowpe *et al.*, 2009; Haq *et al.*, 2015):

$$\Delta\lambda_{1/2} = 2w\left[\frac{N_e}{10^{16}}\right] \quad (4)$$

In the present study, the electron density is determined using the Stark-broadened profile from the atomic tungsten transition at 430.2 nm using Eq. (4). The value of the electron impact parameter for this line is taken from the literature (Nishijima and Doerner, 2015). The Stark-broadened line of WI at 430.2 nm is fitted using the Lorentzian function and is shown in Figure 9a at a delay of 0.5 μs and the fluence of 60 J/cm² as an example. The correlation coefficient for the fitted Lorentzian function, for the measurement of the electron, is found to be 0.99.

The variation in the electron density as a function of delay time for all the four laser fluences is shown in Figure 11b. The electron density is varying from 2.40−1.70 (±0.15), 2.33−1.76 (±0.13), 2.44−1.84 (±0.16), and 2.54−1.82 (±0.07) × 10¹⁷ cm⁻³ as the delay time increases from 0.5 to 5 μs, respectively, in the increasing order of fluence (Surmick and Parigger, 2015).

It is observed from Figures 4, 8, and 9 that the intensity of the spectral lines, the plasma temperature and electron density are falling down with respect to delay time and increase with the increase of laser fluence. The plasma temperature and electron density are found to be maximum at 0.5 μs delay (initial recording time) at each of the incident laser fluence. Immediately after the commencement of the LIP, it starts expanding into the surrounding medium and loses its energy. The overall process of LIB can be divided into three stages: first one is the initial laser-target interaction to form plasma, second one is plasma-laser interaction, and the last stage is plasma cooling and particulates formation (Singh and Thakur, 2007). The rising part of the laser pulse generates the plasma, while the trailing part heats the plasma. During the laser pulse, the plasma expands isothermally, but after the termination of the laser pulse, its expansion is adiabatic, as there is no means to supplement the energy further to the
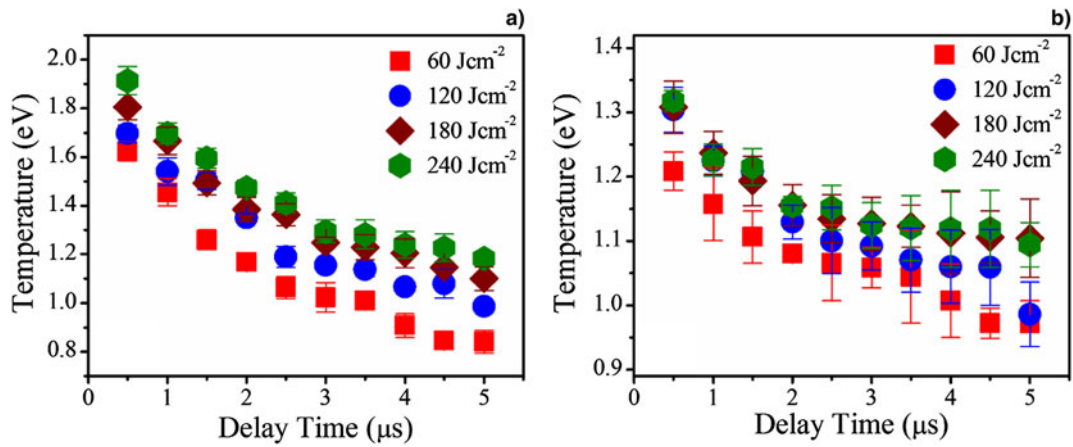
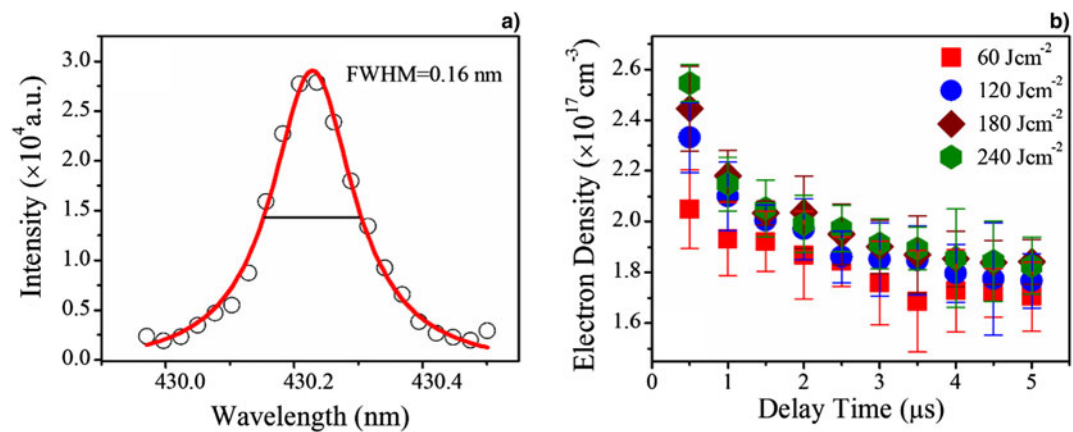**Fig. 8.** Temporal variation of plasma temperature at all the four laser fluences from (a) WII and (b) WI lines.

Fig. 9. Stark-broadened line of WI at 430.2 nm fitted using the Lorentzian profile at a delay time of 0.5 μs for the laser fluence of 60 J/cm² and (b) temporal variation of electron density at all the four laser fluences.
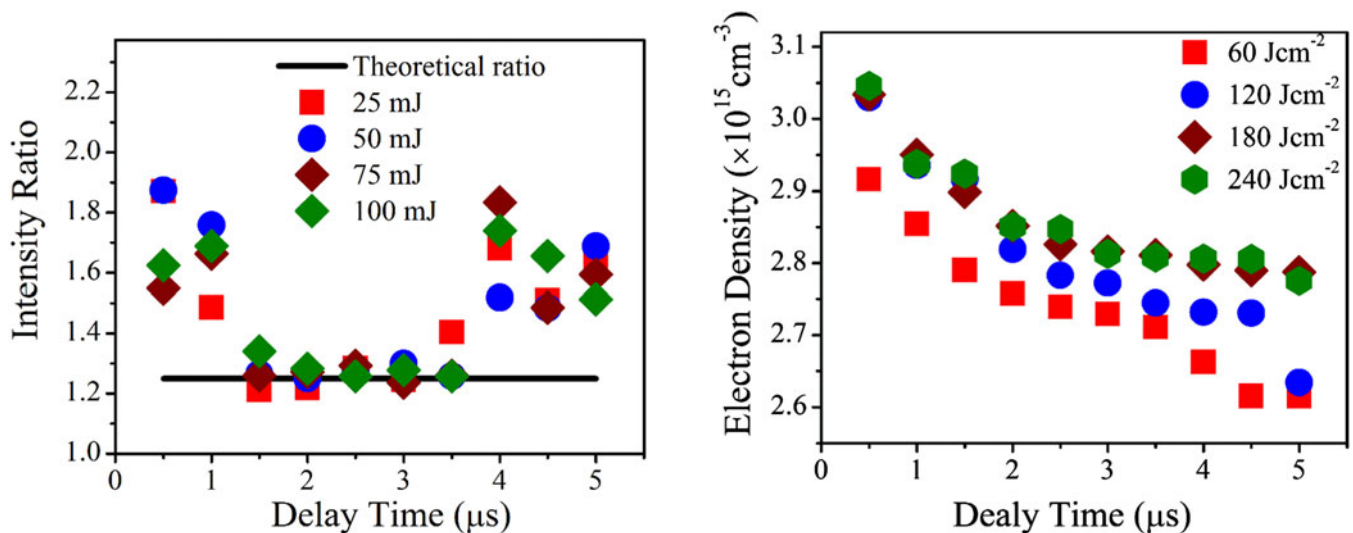

Fig. 10. Comparison of the experimental intensity ratio with the theoretical intensity ratio for optically thin plasma as a function of delay time and laser fluence.
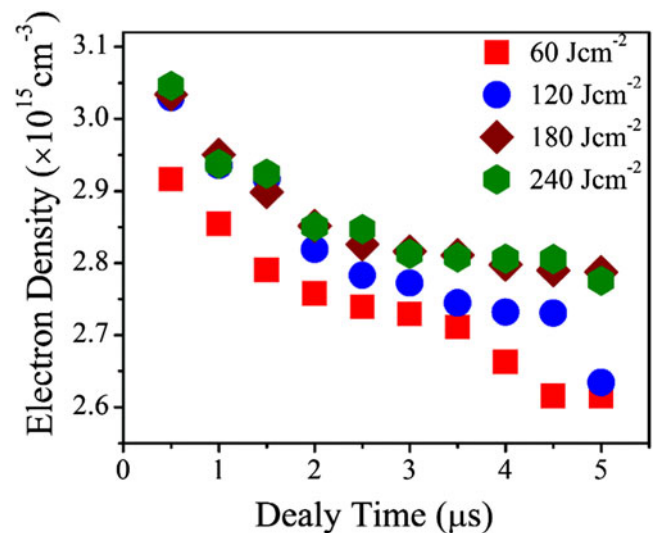
Fig. 11. Temporal evolution of minimum required electron density required from the McWhirter criteria for LTE at various laser fluences.

plasma. Thus, it loses its energy due to thermal conduction to the ambient and target sample, the conversion of the thermal energy to the kinetic energy via work done by the expanding plasma and the various radiative as well as non-radiative processes involved in it along with the collisional mechanism. Due to all these energy dissipative processes with the time, the temperature and electron density fall down (Harilal *et al.*, 2005; Hussein *et al.*, 2013). The emission of radiation from the plasma is interrelated with the plasma temperature and electron density and exhibited the similar trend in temporal behavior as that of plasma parameters (Figs 4, 10, and 11). The fall in plasma parameters is faster during 0.5–1.5 µs as compared with that of the later time of 2–5 µs. The possible reasons behind this are three-body recombination and the effect of surrounding atmosphere particularly at a later stage. In the three-body recombination process, the energy is released due to the recombination of ions and electrons, which compensate the energy loss due to plasma expansion (Shaikh *et al.*, 2006a; Freeman *et al.*, 2013).

The LIP radiation and plasma parameters are strongly influenced by the laser fluence. The target absorbs the energy mainly from the initial rising part of the laser pulse, and this absorption increases with the increase in the laser fluence, thus furnishing the higher plasma temperature and electron density. However, at the laser fluence above the plasma shielding effect (Harilal *et al.*, 1997; Haq *et al.*, 2015), the absorption of energy by the target is curtailed, and thus, the plasma parameters exhibit hardly any variation with the impinging laser fluence. Figures 4, 10, and 11 clearly indicate that the variation in the intensity of the spectral lines, the plasma temperature and electron density with the laser fluence are more prominent up to 180 J/cm², and beyond this fluence, there is not much significant difference in the plasma characteristics with further increase in the laser fluence (Farid *et al.*, 2014; Haq *et al.*, 2015).

Validity of the optical thin condition of plasma

The use of OES for the measurement of plasma temperature and electron number density demands that plasma emission should be optically thin and plasma should be in LTE. Optical thin plasma means that plasma should not absorb its own radiation. If the plasma is not optically thin, then the lines involved in the characterization of plasma undergo self-absorptions. Due to this, the spectral line profile exhibits distorted line shape leading to enormous error in the determination of electron density and plasma temperature. To verify the condition of optically thin plasma in the present case, the theoretical branching ratio is compared with the experimental intensity ratio of the emitted lines. The branching ratio of two atomic lines originating from the same upper energy level is defined by the following equation (Shaikh *et al.*, 2006b; Zhang *et al.*, 2014):

$$\frac{I_1}{I_2} = \frac{g_1 A_1 \lambda_2}{g_2 A_2 \lambda_1} \tag{5}$$

For this, the intensity ratio of atomic transitions of WI at 468.0 and 500.6 nm having the same upper energy level, that is, 3.247 eV is calculated as a function of time at all the four fluences. The theoretical branching ratio from Eq. (5) for these lines is 1.26. The experimental values of the branching ratio are varying from 1.25–1.40, 1.26–1.25, 1.25–1.25, and 1.34–1.25 for the time range of 1–3.5 µs at 60, 120, 180, and 270 J/cm² of the laser fluence, respectively, as shown in Figure 10.

The temporal evolution of the branching ratio shows that the deviation in experimental values is minimum in the delay range of 1–3.5 µs, but for 0.5 and 4–5 µs, there is a large deviation from the theoretical value. Thus, the optimum temporal window in which the plasma can be assumed to be optically thin is 1–3.5 µs.

Validity of LTE in LIP of tungsten

The LIP is of high density and high temperature along with being highly transient and inhomogeneous in nature (Shaikh *et al.*, 2008; Zhang *et al.*, 2014). Due to all these, the total ideal thermodynamic equilibrium state for LIP can never be completely attained. Thus, the concept of LTE is introduced (Cristoforetti *et al.*, 2010b; Zhang *et al.*, 2014). The LTE condition in the plasma is studied under three different conditions (Zhang *et al.*, 2014), that is, the first case, plasma is assumed to be stationary and homogeneous, the second case, it is considered to be transient but homogeneous, and third case, the plasma is regarded as stationary but inhomogeneous. In the first case, in order to satisfy the LTE condition, the collisional processes between electron-atom and electron-ion should be very fast and dominating over the radiative processes, former of which requires a sufficiently large electron density (Shaikh *et al.*, 2008). The lower limit of electron density for which plasma can be described in LTE is given by the McWhirter criterion given by the following equation (Mortazavi *et al.*, 2014; Zhang *et al.*, 2017):

$$N_e \geq 1.6 \times 10^{12} T_e^{1/2} (\Delta E)^3 \tag{6}$$

where N_e (cm^{-3}) is the electron density, and ΔE (eV) is the energy difference between the states expected to be in LTE. The lower limit for electron density in the present case is estimated using energy gap $\Delta E = 2.487$ eV between the ground level and the first excited level of WI-498.2 as a function of delay time and is shown in Figure 11, which varies from 2.91–1.61, 3.02–2.63, 3.03–2.78, and 3.04–2.77 × 10^{15} cm^{-3} for the incident laser fluence of 60, 120, 180, and 270 J/cm², respectively, and this range of minimum electron density is nearly similar for all the laser fluences.

On comparing Figures 9b and 11, it is obvious that the required minimum electron density as per Eq. (6) is less than that of the experimentally estimated for all the four laser fluences, confirming the LTE for LIP of tungsten in the present case.

In the case of inhomogeneous and transient plasma, the temporal evolution of the plasma parameters should be sufficiently slow in order to allow the plasma sufficient time to reach the thermodynamic equilibrium. This requires that the plasma relaxation time, t_{rel}, the time required to establish excitation and ionization equilibrium should be much shorter than the time of variation of plasma parameters, that is (Cristoforetti *et al.*, 2010a),

$$\frac{T_e(t + t_{rel}) - T_e(t)}{T_e(t)} \ll 1 \qquad \frac{N_e(t + t_{rel}) - N_e(t)}{N_e(t)} \ll 1 \tag{7}$$

The relaxation time is estimated by the following equation (Cristoforetti *et al.*, 2010a):

$$t_{rel} = \frac{6.3 \times 10^4}{N_e f_{mn} \langle g \rangle} \Delta E_{nm} (kT_e)^{1/2} \exp\left(\frac{\Delta E_{nm}}{kT_e}\right) \tag{8}$$

where t_{rel} is the relaxation time (s), ΔE_{nm} is the energy difference between the levels, f_{nm} is the transition oscillator strength, g is the
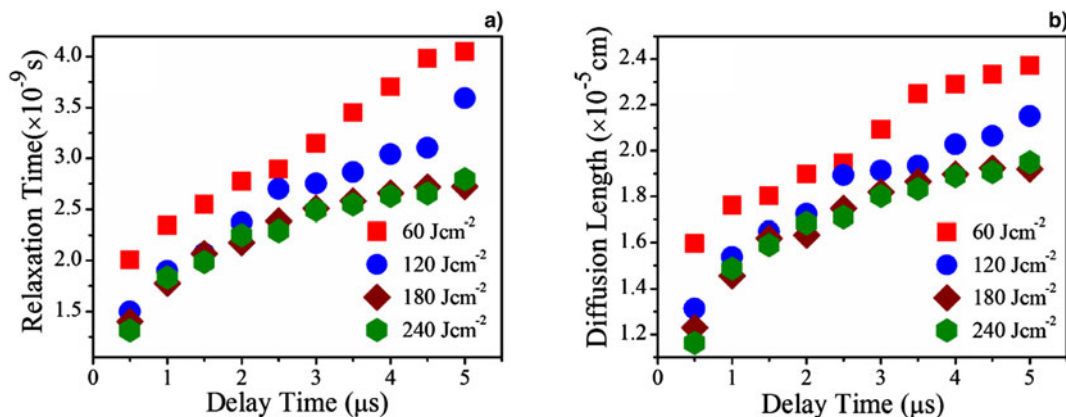
Fig. 12. Assessment of LTE at various delay times as a function of incident laser fluence: (a) relaxation time and (b) diffusion length parameters.

effective gaunt factor, and N_e is the electron density. The WI-498.2 nm transition having $\Delta E_{nm} = 2.487$ eV and $f_{nm} = 0.0046$ is used to estimate the relaxation time. The variation in the relaxation time as a function of delay time with respect to laser pulse is shown in Figure 12a. The relaxation time in the present experimental conditions is found to be of the order of 10^{-9} s, which is much smaller than decay time of plasma parameters, estimated to be of the order of microsecond (Fig. 5a), thus satisfying the second criteria for the LTE condition.

The third condition for LTE demands the diffusion length during the relaxation time should be small compared with the dimension of the plasma (Cristoforetti *et al.*, 2010*a*):

$$\frac{T_e(x) - T_e(x + \Lambda)}{T_e(x)} \ll 1 \quad \frac{N_e(x) - N_e(x + \Lambda)}{N_e(x)} \ll 1 \quad (9)$$

where Λ is the diffusion length (cm) during the relaxation time given by the following equation (Cristoforetti *et al.*, 2010*a*):

$$\Lambda = 1.4 \times 10^{12} \frac{(kT)^{3/4}}{N_e} \left(\frac{\Delta E_{nm}}{M_A f_{nm}}\right)^{1/2} \exp\left(\frac{\Delta E_{nm}}{2kT_e}\right) \quad (10)$$

In Eq. (10), M_A is the atomic mass of element emitting the transition. The variation in the diffusion length as a function of time is shown in Figure 12b and is of the order of 10^{-5} cm. The inhomogeneous plasma will fulfill the LTE condition provided the plasma size is at least 10 times larger than Λ. In the present experimental condition, the size of the plasma is of the order of 10^{-1} cm confirming the validity of the third criteria of LTE.

Conclusions

The temporal evolution of LIP of tungsten in air is studied as a function of incident laser fluence through the LIBS technique. It is observed that plasma emission intensity decreases with time, and atomic lines persist for a longer duration than ionic lines. The temporal evolution of SNR increases with fluence in the temporal window of 0.5–3.5 μs, but beyond this window, it is quite low. The plasma temperature is estimated by carefully selecting several atomic and ionic transitions of tungsten by the Boltzmann plot method. In the temporal window of 0.5–1 μs, the ions are observed to be at a higher temperature compared with that of atoms, while at a later time in the temporal window of 1.5–4 μs, both these possess nearly the same temperature

indicating the coexistence of thermodynamic equilibrium among tungsten atoms and ions. The Stark-broadened profile of WI line at 430.2 nm is exploited for the estimation of electron densities of LIP of tungsten. The emitted line intensities as well as both the plasma parameters initially increases with the increase in laser fluence but saturated at higher fluence due to the plasma shielding effect. The LTE and optical thin condition of LIP are also assessed in the present experimental condition. The temporal evolution of all these parameters indicates that there is need to record the spectrum in a particular time window of 1.5–4 μs and laser fluence so as to have high SNR and validity of the LTE and optical thin condition of LIP. The obtained parameters in the present study may prove to be a sort of reference for the estimation of missing atomic parameters that are essential for spectroscopic study in different experimental conditions.

References

Afif M, Girardeau-Montaut J, Tomas C, Romand M, Charbonnier M, Prakash N, Perez A, Marest G and Frigerio J (1996) In situ surface cleaning of pure and implanted tungsten photocathodes by pulsed laser irradiation. *Applied Surface Science* **96**, 469–473.

Aguilera JA and Aragón C (2004) Characterization of a laser-induced plasma by spatially resolved spectroscopy of neutral atom and ion emissions: comparison of local and spatially integrated measurements. *Spectrochimica Acta Part B: Atomic Spectroscopy* **59**, 1861–1876.

Akram M, Bashir S, Hayat A, Mahmood K, Ahmad R and Khaleeq-U-Rahaman M (2014) Effect of laser irradiance on the surface morphology and laser-induced plasma parameters of zinc. *Laser and Particle Beams* **32**, 119–128.

Almaviva S, Caneve L, Colao F, Fantoni R and Maddaluno G (2012) Laboratory feasibility study of fusion vessel inner wall chemical analysis by laser-induced breakdown spectroscopy. *Chemical Physics* **398**, 228–232.

Amoruso S, Ausanio G, Bruzzese R, Vitiello M and Wang X (2005) Femtosecond laser pulse irradiation of solid targets as a general route to nanoparticle formation in a vacuum. *Physical Review B* **71**, 033406.

Bauer AJR and Buckley SG (2017) Novel applications of laser-induced breakdown spectroscopy. *Applied Spectroscopy* **71**, 553–566.

Bolt H, Barabash V, Krauss W, Linke J, Neu R, Suzuki S, Yoshida N and Team AU (2004) Materials for the plasma-facing components of fusion reactors. *Journal of Nuclear Materials* **329**, 66–73.

Brezinsek S, Loarer T, Philipps V, Esser H, Grünhagen S, Smith R, Felton R, Banks J, Belo P and Boboc A (2013) Fuel retention studies with the ITER-like wall in JET. *Nuclear Fusion* **53**, 083023.

Cabalin L and Laserna J (1998) Experimental determination of laser induced breakdown thresholds of metals under nanosecond Q-switched laser operation. *Spectrochimica Acta Part B: Atomic Spectroscopy* **53**, 723–730.

Chenais-Popovics C, Rancu O, Renaudin P and Gauthier J (1996) X-ray spectroscopy of laser-produced hot dense plasmas. *Physica Scripta* **1996**, 163.

Cortez J, Farias Filho BB, Fontes LM, Pasquini C, Raimundo IM, Pimentel MF and Borba FdSL (2017) A simple device for lens-to-sample distance adjustment in laser-induced breakdown spectroscopy (LIBS). *Applied Spectroscopy* **71**, 634–639.

Cowpe J, Pilkington R, Astin J and Hill A (2009) The effect of ambient pressure on laser-induced silicon plasma temperature, density and morphology. *Journal of Physics D: Applied Physics* **42**, 165202.

Cristoforetti G, De Giacomo A, Dell'Aglio M, Legnaioli S, Tognoni E, Palleschi V and Omenetto N (2010a) Local thermodynamic equilibrium in laser-induced breakdown spectroscopy: beyond the McWhirter criterion. *Spectrochimica Acta Part B: Atomic Spectroscopy* **65**, 86–95.

Cristoforetti G, Lorenzetti G, Legnaioli S and Palleschi V (2010b) Investigation on the role of air in the dynamical evolution and thermodynamic state of a laser-induced aluminium plasma by spatial- and time-resolved spectroscopy. *Spectrochimica Acta Part B: Atomic Spectroscopy* **65**, 787–796.

Davis J, Barabash V, Makhankov A, Plöchl L and Slattery K (1998) Assessment of tungsten for use in the ITER plasma facing components. *Journal of Nuclear Materials* **258**, 308–312.

De Giacomo A and Hermann J (2017) Laser-induced plasma emission: from atomic to molecular spectra. *Journal of Physics D: Applied Physics* **50**, 183002.

Dellasega D, Merlo G, Conti C, Bottani CE and Passoni M (2012) Nanostructured and amorphous-like tungsten films grown by pulsed laser deposition. *Journal of Applied Physics* **112**, 084328.

Díaz D, Molina A and Hahn D (2018) Effect of laser irradiance and wavelength on the analysis of gold- and silver-bearing minerals with laser-induced breakdown spectroscopy. *Spectrochimica Acta Part B: Atomic Spectroscopy* **145**, 86–95.

Eliezer S, Eliaz N, Grossman E, Fisher D, Gouzman I, Henis Z, Pecker S, Horovitz Y, Fraenkel M and Maman S (2005) Nanoparticles and nanotubes induced by femtosecond lasers. *Laser and Particle Beams* **23**, 15–19.

Ershov-Pavlov E, Katsalap KY, Stepanov K and Stankevich YA (2008) Time-space distribution of laser-induced plasma parameters and its influence on emission spectra of the laser plumes. *Spectrochimica Acta Part B: Atomic Spectroscopy* **63**, 1024–1037.

Farid N, Harilal S, El-Atwani O, Ding H and Hassanein A (2013) Experimental simulation of materials degradation of plasma-facing components using lasers. *Nuclear Fusion* **54**, 012002.

Farid N, Harilal S, Ding H and Hassanein A (2014) Emission features and expansion dynamics of nanosecond laser ablation plumes at different ambient pressures. *Journal of Applied Physics* **115**, 033107.

Federici G, Zhitlukhin A, Arkhipov N, Giniyatulin R, Klimov N, Landman I, Podkovyrov V, Safronov V, Loarte A and Merola M (2005) Effects of ELMs and disruptions on ITER divertor armour materials. *Journal of Nuclear Materials*, 684–690.

Freeman J, Harilal S, Diwakar P, Verhoff B and Hassanein A (2013) Comparison of optical emission from nanosecond and femtosecond laser produced plasma in atmosphere and vacuum conditions. *Spectrochimica Acta Part B: Atomic Spectroscopy* **87**, 43–50.

Freeman J, Diwakar P, Harilal S and Hassanein A (2014) Improvements in discrimination of bulk and trace elements in long-wavelength double pulse LIBS. *Spectrochimica Acta Part B: Atomic Spectroscopy* **102**, 36–41.

Fu H, Dong F, Ni Z and Wang J (2016) The influence of acquisition delay for calibration-free laser-induced breakdown spectroscopy. *Applied Spectroscopy* **70**, 405–415.

Fukuda M, Hasegawa A, Tanno T, Nogami S and Kurishita H (2013) Property change of advanced tungsten alloys due to neutron irradiation. *Journal of Nuclear Materials* **442**, S273–S276.

Ganeev R (2007) High-order harmonic generation in a laser plasma: a review of recent achievements. *Journal of Physics B: Atomic, Molecular and Optical Physics* **40**, R213.

Gao X, Liu L, Song C and Lin J (2015) The role of spatial confinement on nanosecond YAG laser-induced Cu plasma. *Journal of Physics D: Applied Physics* **48**, 175205.

Haq S, Ahmat L, Mumtaz M, Shakeel H, Mahmood S and Nadeem A (2015) Spectroscopic studies of magnesium plasma produced by fundamental and second harmonics of Nd:YAG laser. *Physics of Plasmas* **22**, 083504.

Harilal S, Bindhu C, Issac RC, Nampoori V and Vallabhan C (1997) Electron density and temperature measurements in a laser produced carbon plasma. *Journal of Applied Physics* **82**, 2140–2146.

Harilal S, O'shay B, Tillack MS and Mathew MV (2005) Spectroscopic characterization of laser-induced tin plasma. *Journal of Applied Physics* **98**, 013306.

Harilal S, O'Shay B, Tao Y and Tillack MS (2006) Ambient gas effects on the dynamics of laser-produced tin plume expansion. *Journal of Applied Physics* **99**, 083303.

Harilal S, Sizyuk T, Hassanein A, Campos D, Hough P and Sizyuk V (2011) The effect of excitation wavelength on dynamics of laser-produced tin plasma. *Journal of Applied Physics* **109**, 063306.

Harilal S, Farid N, Hassanein A and Kozhevin V (2013) Dynamics of femtosecond laser produced tungsten nanoparticle plumes. *Journal of Applied Physics* **114**, 203302.

Hussein A, Diwakar P, Harilal S and Hassanein A (2013) The role of laser wavelength on plasma generation and expansion of ablation plumes in air. *Journal of Applied Physics* **113**, 143305.

Kawakami Y and Ozawa E (2002) Tungsten microcone arrays grown using nanosecond pulsed-Nd:YAG laser in a low-pressure He-gas atmosphere. *Applied Physics A* **74**, 59–61.

Kubkowska M, Gasior P, Rosinski M, Wolowski J, Sadowski M, Malinowski K and Skladnik-Sadowska E (2009) Characterisation of laser-produced tungsten plasma using optical spectroscopy method. *The European Physical Journal D* **54**, 463–466.

Lazzari C, De Rosa M, Rastelli S, Ciucci A, Palleschi V and Salvetti A (1994) Detection of mercury in air by time-resolved laser-induced breakdown spectroscopy technique. *Laser and Particle Beams* **12**, 525–530.

Le Drogoff B, Margot J, Vidal F, Laville S, Chaker M, Sabsabi M, Johnston T and Barthélemy O (2004) Influence of the laser pulse duration on laser-produced plasma properties. *Plasma Sources Science and Technology* **13**, 223.

Li X, Wei W, Wu J, Jia S and Qiu A (2013) The Influence of spot size on the expansion dynamics of nanosecond-laser-produced copper plasmas in atmosphere. *Journal of Applied Physics* **113**, 243304.

Lowndes DH, Geohegan D, Puretzky A, Norton D and Rouleau C (1996) Synthesis of novel thin-film materials by pulsed laser deposition. *Science* **273**, 898–903.

Mal E, Junjuri R, Gundawar MK and Khare A (2019) Optimization of temporal window for application of calibration free-laser induced breakdown spectroscopy (CF-LIBS) on copper alloys in air employing a single line. *Journal of Analytical Atomic Spectrometry* **34**, 319-330.

Mercadier L, Hermann J, Grisolia C and Semerok A (2011) Analysis of deposited layers on plasma facing components by laser-induced breakdown spectroscopy: towards ITER tritium inventory diagnostics. *Journal of Nuclear Materials* **415**, S1187–S1190.

Mortazavi S, Parvin P, Pour MM, Reyhani A, Moosakhani A and Moradkhani S (2014) Time-resolved evolution of metal plasma induced by Q-switched Nd:YAG and ArF-excimer lasers. *Optics & Laser Technology* **62**, 32–39.

Mostako A, Rao C and Khare A (2011) Mirrorlike pulsed laser deposited tungsten thin film. *Review of Scientific Instruments* **82**, 013101.

Multari RA, Foster LE, Cremers DA and Ferris MJ (1996) Effect of sampling geometry on elemental emissions in laser-induced breakdown spectroscopy. *Applied Spectroscopy* **50**, 1483–1499.

Neu R, Brezinsek S, Beurskens M, Bobkov V, de Vries P, Giroud C, Joffrin E, Kallenbach A, Matthews G and Mayoral M-L (2013) Tungsten experiences in ASDEX Upgrade and JET. *2013 IEEE 25th Symposium on Fusion Engineering (SOFE)*, 10–14 June 2013, San Francisco, CA, USA. IEEE, pp. 1–8.

Nishijima D and Doerner R (2015) Stark width measurements and Boltzmann plots of WI in nanosecond laser-induced plasmas. *Journal of Physics D: Applied Physics* **48**, 325201.

NIST database. https://www.nist.gov.

Philipps V (2011) Tungsten as material for plasma-facing components in fusion devices. *Journal of Nuclear Materials* **415**, S2–S9.

Philipps V, Malaquias A, Hakola A, Karhunen J, Maddaluno G, Almaviva S, Caneve L, Colao F, Fortuna E and Gasior P (2013) Development of laser-based techniques for in situ characterization of the first wall in ITER and future fusion devices. *Nuclear Fusion* **53**, 093002.

Piip K, De Temmerman G, van der Meiden H, Lissovski A, Karhunen J, Aints M, Hakola A, Paris P, Laan M and Likonen J (2015) LIBS analysis of tungsten coatings exposed to Magnum PSI ELM-like plasma. *Journal of Nuclear Materials* **463**, 919–922.

Pitts R, Bardin S, Bazylev B, van den Berg M, Bunting P, Carpentier-Chouchana S, Coenen J, Corre Y, Dejarnac R and Escourbiac F (2017) Physics conclusions in support of ITER W divertor monoblock shaping. *Nuclear Materials and Energy* **12**, 60–74.

P.L. Smith, C. Heise, J.R. Esmond, R.L. Kurucz. Atomic spectral line database from CD-ROM 23 of R. L. Kurucz. https://www.cfa.harvard.edu/amp/ampdata/kurucz23/sekur.html.

Radziemski LJ and Cremers DA (2006) *Handbook of Laser Induced Breakdown Spectroscopy*, Vol. **1**. West Sussex, England: John Wiley & Sons, pp. 1–4.

Russo RE (1995) Laser ablation. *Applied Spectroscopy* **49**, 14A–28A.

Shaikh NM, Hafeez S, Rashid B, Mahmood S and Baig M (2006a) Optical emission studies of the mercury plasma generated by the fundamental, second and third harmonics of a Nd:YAG laser. *Journal of Physics D: Applied Physics* **39**, 4377.

Shaikh NM, Rashid B, Hafeez S, Jamil Y and Baig M (2006b) Measurement of electron density and temperature of a laser-induced zinc plasma. *Journal of Physics D: Applied Physics* **39**, 1384.

Shaikh NM, Hafeez S, Kalyar M, Ali R and Baig M (2008) Spectroscopic characterization of laser ablation brass plasma. *Journal of Applied Physics* **104**, 103108.

Singh JP and Thakur SN (2007) *Laser-Induced Breakdown Spectroscopy*. Amsterdam, The Netherlands/Oxford, UK: Elsevier.

Skrodzki PJ, Becker JR, Diwakar PK, Harilal SS and Hassanein A (2016) A comparative study of single-pulse and double-pulse laser-induced breakdown spectroscopy with uranium-containing samples. *Applied Spectroscopy* **70**, 467–473.

Surmick D and Parigger C (2015) Electron density determination of aluminium laser-induced plasma. *Journal of Physics B: Atomic, Molecular and Optical Physics* **48**, 115701.

Suslova A, El-Atwani O, Harilal S and Hassanein A (2015) Material ejection and surface morphology changes during transient heat loading of tungsten as plasma-facing component in fusion devices. *Nuclear Fusion* **55**, 033007.

Thaury C and Quéré F (2010) High-order harmonic and attosecond pulse generation on plasma mirrors: basic mechanisms. *Journal of Physics B: Atomic, Molecular and Optical Physics* **43**, 213001.

Wang QH, Kalantar-Zadeh K, Kis A, Coleman JN and Strano MS (2012) Electronics and optoelectronics of two-dimensional transition metal dichalcogenides. *Nature Nanotechnology* **7**, 699.

Wermer L, Lefkowitz JK, Ombrello T, Bak MS and Im S-K (2018) Spatiotemporal evolution of the plasma from dual-pulsed laser-induced breakdown in an atmospheric air. *Plasma Sources Science and Technology* **27**, 015012.

White J, Dunne P, Hayden P, O'Reilly F and O'Sullivan G (2007) Optimizing 13.5 nm laser-produced tin plasma emission as a function of laser wavelength. *Applied Physics Letters* **90**, 181502.

Winefordner JD, Gornushkin IB, Correll T, Gibb E, Smith BW and Omenetto N (2004) Comparing several atomic spectrometric methods to the super stars: special emphasis on laser induced breakdown spectrometry, LIBS, a future super star. *Journal of Analytical Atomic Spectrometry* **19**, 1061–1083.

Zehra K, Bashir S, Hassan S, Ahmed QS, Akram M and Hayat A (2017) The effect of nature and pressure of ambient environment on laser-induced breakdown spectroscopy and ablation mechanisms of Si. *Laser and Particle Beams* **35**, 492–504.

Zhang S, Wang X, He M, Jiang Y, Zhang B, Hang W and Huang B (2014) Laser-induced plasma temperature. *Spectrochimica Acta Part B: Atomic Spectroscopy* **97**, 13–33.

Zhang D, Chen A, Wang X, Li S, Wang Y, Sui L, Jiang Y and Jin M (2017) Enhancement mechanism of femtosecond double-pulse laser-induced Cu plasma spectroscopy. *Optics & Laser Technology* **96**, 117–122.